buildings

Article

Identification of Damage in Planar Multistory Reinforced Concrete Frames Developing a Beam-Sway Plastic Mechanism Using the "M and P" Technique

Triantafyllos K. Makarios * and Athanasios P. Bakalis

Institute of Structural Analysis and Dynamics of Structures, School of Civil Engineering, Aristotle University of Thessaloniki, GR-54124 Thessaloniki, Greece; abakalis@civil.auth.gr
* Correspondence: makariostr@civil.auth.gr

Abstract: The effectiveness of a recently proposed methodology for the identification of damage in planar, multistory, reinforced concrete (RC) moment frames, which develop a plastic yield mechanism on their beams, is showcased here via the examining of a group of such existing multistory frames with three or more unequal spans. According to the methodology, the diagram of the instantaneous eigenfrequencies of the frame in the nonlinear regime is drawn as a function of the inelastic seismic roof displacement by the performance of a sequence of pushover and instantaneous modal analyses with gradually increasing target displacement. Using this key diagram, the locations of severe seismic damage in an existing moment frame can be evaluated if the instantaneous fundamental eigenfrequency of the damaged frame, at an analysis step within the nonlinear area, is known in advance by "the monitoring and the identification of frequencies" using a local network of uniaxial accelerometers. This is a hybrid technique because both procedures, the instrumental monitoring of the structure and the pushover analysis on the frame (M and P technique), are combined. A ductile, five-story, planar RC moment frame with three unequal spans is evaluated in this paper by the M and P technique. The results show that the seismic roof displacement, the lateral stiffness matrix, and, finally, the damage image of this existing frame, are fully compatible with the eigenfrequencies identified by the monitoring and are calculated with high accuracy.

Keywords: damage identification; instantaneous eigenfrequencies diagram; pushover capacity curve; seismic target displacement; beam-sway plastic mechanism

check for updates

Citation: Makarios, T.K.; Bakalis, A.P. Identification of Damage in Planar Multistory Reinforced Concrete Frames Developing a Beam-Sway Plastic Mechanism Using the "M and P" Technique. *Buildings* **2023**, *13*, 2316. https://doi.org/10.3390/buildings13092316

Academic Editor: Marco Di Ludovico

Received: 14 August 2023
Revised: 2 September 2023
Accepted: 10 September 2023
Published: 12 September 2023

1. Introduction

The identification of damage in reinforced concrete (RC) structures can be conducted by the detection of variations in their dynamic characteristics with reference to the undamaged state. This identification process contributes to the creation of reliable structural models for advanced nonlinear analyses of the inherent building seismic capacity. To detect the eigenfrequencies (and mode shapes) of existing RC structures, instrumental monitoring of the structure by an installed local multichannel network system of accelerometers is necessary; then, an analytic processing of the recorded response should be performed by using the various stochastic and deterministic procedures that were developed in the past. For instance, the "frequency domain decomposition" technique was used in "operational modal analysis" [1–4]. Also, much information about ambient vibration monitoring can be found in the book by Wenzel and Pichler [5]. Moreover, several techniques have been proposed using "stochastic subspace identification". These techniques are based on the classic books by Overschee and De Moor [6], in which they directly fit the measured responses to the parametric models. Three distinct algorithms have been used in stochastic subspace techniques: principal component, canonical variate analysis algorithms, and the unweighted principal component. In all cases, random data analysis and operational modal analysis are the main field of analysis of the recorded accelerograms [7–9]. Based on the aforementioned techniques, the "modal time-histories method" was proposed [10]; this method is suitable for structures subjected to earthquake ground excitation at their bases or structures loaded with strong wind pressure. Using the "modal time-histories method", eigenfrequencies, mode shapes and modal damping ratios have been calculated in the linear domain in various structures [11]. Another important work on the detection of damage in structures was proposed by Zimmerman and Kaouk [12,13]. This is the so-called minimum rank perturbation theory (MRPT), in which a non-zero entry in the damage vector is interpreted as an indicator of the damage location. Also, another technique was developed by Domaneschi et al. [14,15], in which the discontinuity of the forms of mode shapes was used. One more technique, which uses an artificial neural network, was developed by Nazari and Baghalian [16] for simple symmetric beams. Moreover, the idea of the damage stiffness matrix is presented in interesting works, such those of Peeters [3], Amani et al. [17], and Zhang et al. [18]. It is also worth mentioning the recent research efforts by Reuland et al. [19], which led to a comprehensive review of data-driven damage indicators for rapid seismic structural health monitoring, as well as those by Martakis et al. [20], which considered a combination of traditional structural health monitoring techniques with novel machine learning tools. With regard to the rapid spread and application of machine learning (ML), such as artificial neural networks (ANN), in structural engineering, some recent research works in this field are mentioned that consider different types of loading on structures [21–25]. Some other works combine structural health monitoring techniques with pushover analysis to detect damage in structural elements [26] and in frame structures [27]. In [28], damage in steel–concrete composite beams is identified using acoustic emission (AE) measurements. Also, some other works investigate the damage in terms of the mechanical behavior of various strengthened structural elements with different combined loading conditions [29] or after fire exposure [30] and the progressive collapse resistance of strengthened structural elements in multistory RC frames [31,32].

However, detecting the location and the severity of damage in the structure, as well as the significance of the damage, is still an open issue for investigation. To fill a significant part of this gap, an alternative, hybrid procedure for the damage identification in existing planar RC frames has been developed recently by Makarios [33], mainly for the case of seismic loading or wind loading. The last methodology is based, on the one hand, on the development of eigenfrequency curves by performing two pushover analyses in a suitable nonlinear model of the planar moment frame; on the other hand, it is based on the fundamental eigenfrequency (or on the first to the third eigenfrequencies) of the damaged frame, which is (or are) identified by the instrumental monitoring of its structural integrity. Using the fundamental eigenfrequency of the damaged moment frame identified by the instrumental monitoring, all the other higher eigenfrequencies of the moment frame are determined from the diagram of the instantaneous eigenfrequencies of the frame in the nonlinear regime (namely the key diagram). Furthermore, the modal shapes of the damaged frame are determined by instantaneous modal analysis (at the examined step of pushover analysis), where all the calculations are performed in the examined step of the nonlinear area of analysis. Lastly, the damage stiffness matrix of the moment frame is calculated at the examined step to consider all the plastic hinges and the degradation of the member stiffness; therefore, it determines the extent of the damage to the moment frame. Finally, the damage image of the planar RC moment frame, i.e., the location and the magnitude of damage, is obtained from the state of the developed plastic hinges at the corresponding step of pushover analysis. In planar frames, two pushover analyses are performed, the first one along the positive direction and the second one along the negative direction. In both analyses, the floor lateral forces are distributed triangularly (or according to the first mode shape) in the height.

In order to verify the recently proposed methodology mentioned above [33], in frames that develop a beam-sway plastic mechanism, a suitable extended parametric analysis is conducted. In more detail, a group of existing ductile, multistory, multi-span, planar RC frames with various lengths and story heights is examined in this paper in order to determine the damage state; here, a numerical example of a five-story RC moment frame with three unequal spans is presented. All the steps of the proposed methodology (which we call the "M and P" technique in this paper, where M means "Monitoring" and P means "Pushover") are clearly presented in the corresponding section below and applied during the presentation of the numerical example. The article focuses, on the one hand, on the determination of the eigenfrequency curves of the damaged moment frame as a function of the seismic roof displacement, which are drawn by performing a sequence of pushover and instantaneous modal analyses with gradually increasing target displacement; on the other hand, the article focuses on the evaluation of the damage stiffness matrix of the moment frame. In addition, a new load pattern appropriate for tall multistory frames is incorporated in the pushover analysis to take account of the effects of higher modes in the distribution of damage along the height of the frame. Finally, for each case, the damage matrix of the frame is calculated, and the damage image of the frame is illustrated.

Therefore, by using the present methodology, the identification of damage (location and severity) in planar RC frames which develop a beam-sway plastic mechanism can be successfully accomplished numerically by combining the results of monitoring methods with those of pushover analysis. This is an alternative, hybrid technique for damage detection in ductile frame structures, the accuracy of which is ensured by "the monitoring and the identification of frequencies". It is therefore a self-evident process. In the present work, it is shown that for a given damage image in an existing, ductile, frame structure, the stiffness matrix of the healthy state of the structure changes, resulting in a change in the eigenfrequencies of the structure which are identified experimentally by the monitoring procedure. Then, using the key diagram of the method, the seismic roof displacement of the building is determined, which, on the one hand, corresponds to the damage image, and, on the other hand, ensures the same values of eigenfrequencies as those measured in the field.

2. Materials and Methods

The free vibration differential equation of motion of a multi-degree-of-freedom system (MDOF) without damping due to an initial forced displacement or velocity is:

$$\mathbf{m}\ddot{\mathbf{u}}(\mathrm{t}) + \mathbf{k}_o\mathbf{u}(\mathrm{t}) = 0 \tag{1}$$

where $\mathbf{m}$ is the mass matrix of the frame and $\mathbf{k}_o$ is the stiffness matrix of the frame, while $\mathbf{u}(\mathrm{t})$ and $\ddot{\mathbf{u}}(\mathrm{t})$ are the time-varying displacement and acceleration vectors of the system, respectively.

Next, it is assumed that this is an existing system that presents a damage image due to any cause. Then, the stiffness matrix at any time step i will change by $\mathbf{\Delta k}_i$; so, it follows that:

$$\mathbf{k}_i = \mathbf{k}_o - \mathbf{\Delta k}_i \tag{2}$$

where $\mathbf{\Delta k}_i$ is the damage stiffness matrix.

Moreover, the instantaneous mode shapes at each inelastic i-step of the analysis can be defined if a modal linear analysis is performed using the instantaneous stiffness matrix $\mathbf{k}_i$, which includes the damage effects on stiffness. Therefore, the equation of motion is rewritten as:

$$\mathbf{m}\ddot{\mathbf{u}}(\mathrm{t}) + (\mathbf{k}_o - \mathbf{\Delta k}_i)\mathbf{u}(\mathrm{t}) = 0 \tag{3}$$

That is, a modal analysis is performed using the inelastic response of the frame structure at the i-step as the initial condition. Hence, considering that the mass matrix $\mathbf{m}$ does not vary, the eigenvalue problem at the inelastic i-step is written as:

$$\left[(\mathbf{k}_o - \mathbf{\Delta k}_i) - \omega_i^2\mathbf{m}\right]\boldsymbol{\varphi}_i = 0 \tag{4}$$

where ω_i (rad/s) is the instantaneous eigenvalues and $\boldsymbol{\varphi}_i$ is the instantaneous mode shape vectors of the frame structure at the inelastic *i*-step of the analysis. The solution of the eigenvalue problem is given by setting the following determinant to zero and finding the roots ω_i^2 of the resulting algebraic equation:

$$\det\left[(\mathbf{k}_o - \mathbf{\Delta k}_i) - \omega_i^2\mathbf{m}\right] = 0 \tag{5}$$

Then, the instantaneous mode shape vector $\boldsymbol{\varphi}_{i,g}$ can be calculated by Equation (4) for each value of $\omega_{i,g}^2$, where $g = 1, 2, 3, \ldots N$ in an N-degrees-of-freedom system. Moreover, with a known eigenvalue $\omega_{i,g}^2$, Equation (4) is pre-multiplied by $\boldsymbol{\varphi}_{i,g}^T$:

$$\boldsymbol{\varphi}_{i,g}^T \left[(\mathbf{k}_o - \mathbf{\Delta k}_i) - \omega_{i,g}^2\mathbf{m}\right]\boldsymbol{\varphi}_{i,g} = 0 \tag{6}$$

Rearranging the terms in Equation (6), it can be rewritten as follows:

$$\boldsymbol{\varphi}_{i,g}^T\mathbf{\Delta k}_i\boldsymbol{\varphi}_{i,g} = \boldsymbol{\varphi}_{i,g}^T\,\mathbf{k}_o\,\boldsymbol{\varphi}_{i,g} - \omega_{i,g}^2\boldsymbol{\varphi}_{i,g}^T\mathbf{m}\boldsymbol{\varphi}_{i,g} \tag{7}$$

It is noted that it is impossible to identify the instantaneous frequency $\omega_{i,g}$ and the instantaneous mode shape vector $\boldsymbol{\varphi}_{i.g}$ of the structure at the inelastic *i*-step by analysis of the records (time-history analysis with accelerograms) using the random data processing since these procedures require the existence of a sufficient time window, where the eigenfrequencies remain constant. Instead, the obtained records by an installed monitoring multichannel network system of accelerometers must come from the ambient vibration of an existing (with damage) calm structure, without motion. Therefore, if $\omega_{i,g}$, $\boldsymbol{\varphi}_{i,g}, \mathbf{k}_o$, $\mathbf{\Delta k}_i, \mathbf{m}$ are known by the recently proposed methodology [33], then Equation (7) can be used at the end for verification reasons.

In summary, the recently proposed methodology [33] on multistory planar RC frames, using a hybrid technique (that we call the "M and P" technique, where M means "Monitoring" and P means "Pushover") that combines an identification system and a numerical model, consists of the following phases:

(a) The fundamental eigenfrequency f_1 of the existing damaged structure is identified by monitoring with a local network of uniaxial accelerometers located at the characteristic positions along the degrees of freedom of the system. Note that up to the first three eigenfrequencies can be found using the monitoring method.

(b) A suitable numerical nonlinear model of the structure is obtained, and a sequence of separate pushover analyses are performed, targeting each time at a gradual increasing roof displacement $u_{top,i}$. For each target displacement, two pushover analyses are performed, with positive and negative floor forces, leading to the drawing of the capacity curves of the structure in terms of base shear and roof displacement. Figure 1 presents the general form of the capacity curve of a structure in terms of base shear V_o and roof displacement u_{top}, together with the idealized elasto-perfectly plastic force–displacement relationship which defines the idealized yield point (u_y, V_{oy}) of the structure and the effective (secant) stiffness at yield. In addition, various performance levels of the structure are presented in the figure which correspond to different roof displacements $u_{,i}$. The near-collapse state of the structure appears at the ultimate target (roof) displacement, $u_{,ult}$. Regarding the floor lateral force pattern used in pushover analysis, the triangular or the first mode pattern of forces is suitable for building structures up to four floors. For higher buildings, an additional second-floor force pattern is proposed with a unit base shear (V_o), in which an additional force equal to $0.20{\cdot}V_o$ is applied at the top floor [34], and the rest of the base shear (namely the $0.80{\cdot}V_o$) is distributed (in floor forces) according to the triangular or to the first mode pattern. The goal here is to consider the higher mode effects of tall buildings in the linear and nonlinear area, which can be significant, especially for more flexible structures, such as moment frames. Another important point in the application of pushover analysis is that P-D effects should always be considered in the nonlinear area, especially for frame structures which are more flexible.

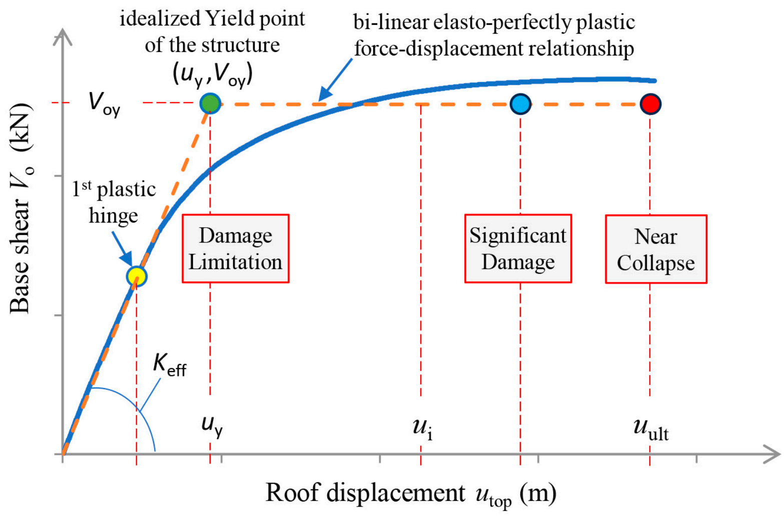

Figure 1. General form of the pushover capacity curve of a multistory planar RC frame structure, with target displacement that corresponds to the NC state.

(c) By performing modal analysis at the last step of each pushover analysis with increasing roof (target) displacement $u_{top,i}$, i.e., by using in modal analysis the stiffness matrix of the damaged structure obtained at the last step of each pushover analysis, the diagram of the instantaneous (step) cyclic eigenfrequencies $f_{N,i}$ (in Hz) of the damaged structure is drawn as a function of the roof displacement $u_{top,i}$ of the structure. The general form of such a diagram is depicted in Figure 2. In this diagram, which is the novel key point of the proposed methodology, the value of the inelastic roof displacement $u_{top,i}$ is the abscissa and the value of the eigenfrequencies $f_{N,i}$ of the damaged structure is the ordinate. With this diagram, the seismic inelastic roof displacement u_i of an existing damaged RC frame can be found by inserting the fundamental eigenfrequency f_1 which was identified by the monitoring in phase (a). This is described in the subsequent phase.

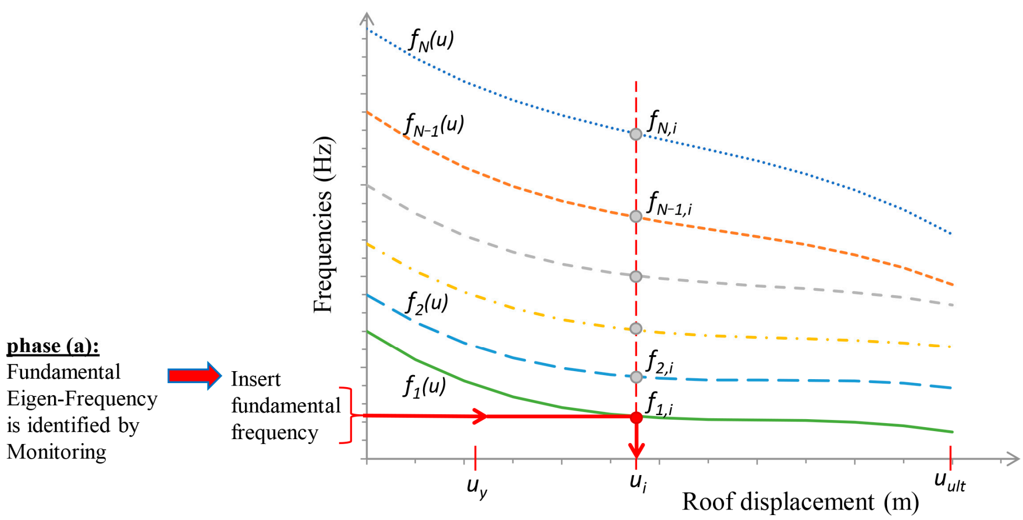

Figure 2. General form of the instantaneous eigenfrequencies diagram, in the nonlinear area. This diagram is calculated according to phase (c) of the present methodology.

It is emphasized that the sequence of pushover and instantaneous modal analyses of the structure, targeting each time at a gradual increasing roof displacement $u_{top,i}$, should be performed in a nonlinear model of the structure with discrete values $E_c I_{eff,i}$ (E_c is the elastic modulus of concrete) of the effective bending stiffness of the RC structural elements. This should be performed because of the different level of stiffness degradation at each target displacement $u_{top,i}$ due to the different damage states (cracking along the entire length of the elements). The damage states correspond to various performance levels: undamaged (health) state, first yield (first plastic hinge formation), damage limitation (DL), significant damage (SD), near collapse (NC), and all the intermediate ones. Hence, an effective stiffness scenario in terms of the effective moment of inertia ratio $I_{eff,i}/I_g$ (where I_g is the moment of inertia of the geometric section) must be prepared before performing pushover and modal analyses, as a function of the mean (chord) rotation of the frame structure, $\theta_{pr,i}$ (in rad), where the subscript *pr,i* refers to the chord rotation profile of the moment frame at the examined roof (target) displacement $u_{t,top,i}$. This is equal to $\theta_{pr,i} = u_{t,top,i}/H_{tot}$, where H_{tot} is the total building height (Figure 3).

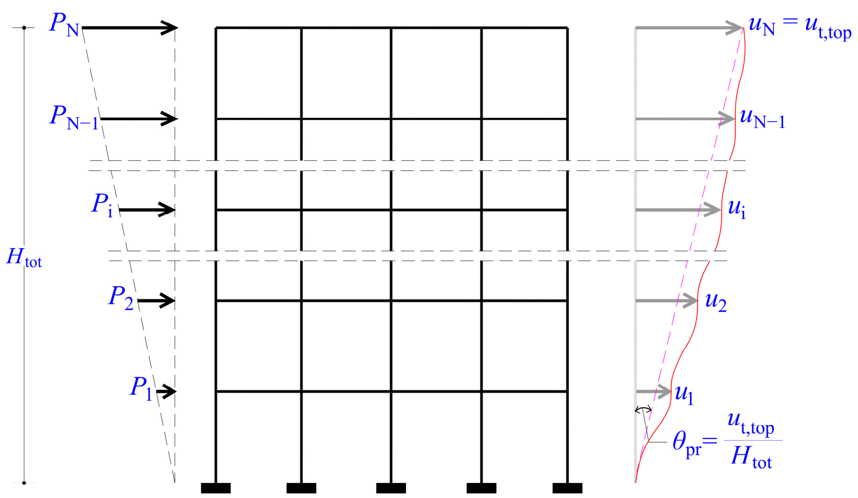

Figure 3. The profile angle θ_{pr} of the frame structure in pushover analysis with floor lateral forces.

As shown in Figure 4, the effective moment of inertia $I_{eff,i}$ of the RC structural elements (as the mean value for their two end-sections) that corresponds to the NC performance level is too low, and it can be calculated from an equation given in EN 1998-3 [35]:

$$E_c I_{\text{eff}} = \frac{M_p \cdot L_v}{3 \cdot \theta_y} \tag{8}$$

where M_p is the plastic moment of the section determined through an elastoplastic idealization of the moment–curvature diagram M-φ of the section; L_v is the shear span of the RC element taken to be equal to the half-clear length of the element [22,23]; and θ_y is the available chord rotation of the shear length of the element at the yield state that is given approximately by Equation (A.10) of Eurocode EN 1998-3. The rationale behind Equation (8), which is clearly based on the elasticity theory, is presented in Figure 5 [36]. The effective bending stiffness of the shear span $L_v = M/V$ (where M is the bending moment and V is the shear force) in a bilinear force–deformation model of an RC element under monotonic loading is the secant stiffness of the shear span to the element yield point. Therefore, considering the clear length of each RC element as a structural cluster of two cantilevers (with opposite bending), with lengths equal to the shear span L_v that corresponds to each extreme critical end section, the effective moment of inertia of the structural element is obtained as the average of the corresponding values of the two shear spans in the positive and negative bending. If it is assumed that both the end sections of all the RC elements develop plastic hinges at the NC state, then the secant (effective) stiffness to the yield point according to Equation (8) is determined [35,36]. It is noted that the consideration of a full plastic mechanism in an RC building at the NC performance level is a fictitious state since usually there are several sections of various structural elements that have not yielded. Despite this fact, EN 1998-3 imposes these low values of the secant (effective) bending stiffness at the yield on all the RC structural elements in order to perform nonlinear analysis that targets not just the NC performance level but also all the other higher performance levels, from DL to NC. This is performed in order to be on the safe side with regard to the calculation of the displacements since the building is more flexible. Hence, this concept is adopted in our present methodology, and this is the main assumption of the present article.

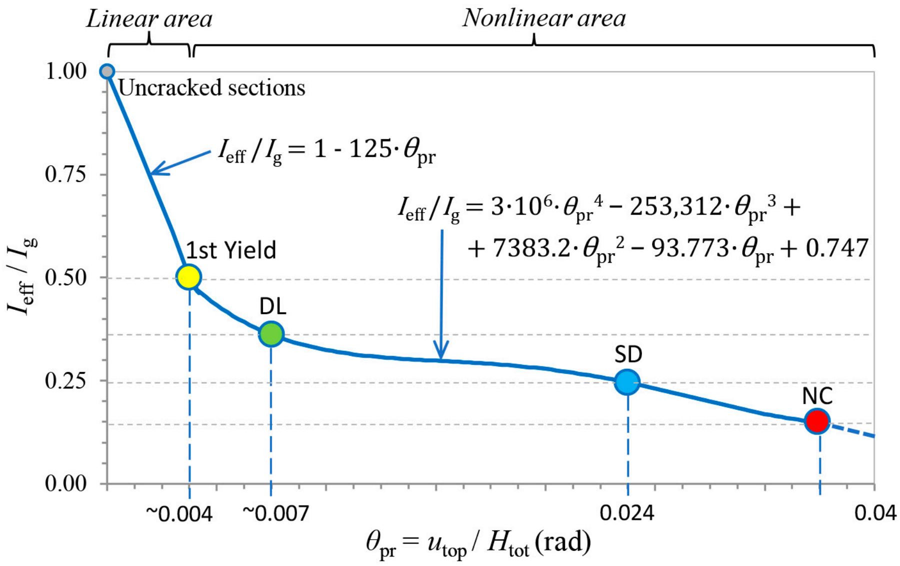

Figure 4. Effective moment of inertia ratio I_{eff}/I_g with reference to the geometric moment of inertia I_g of RC structural elements at discrete damage states as a function of the mean (chord) rotation of the frame structure θ_{pr} (rad).

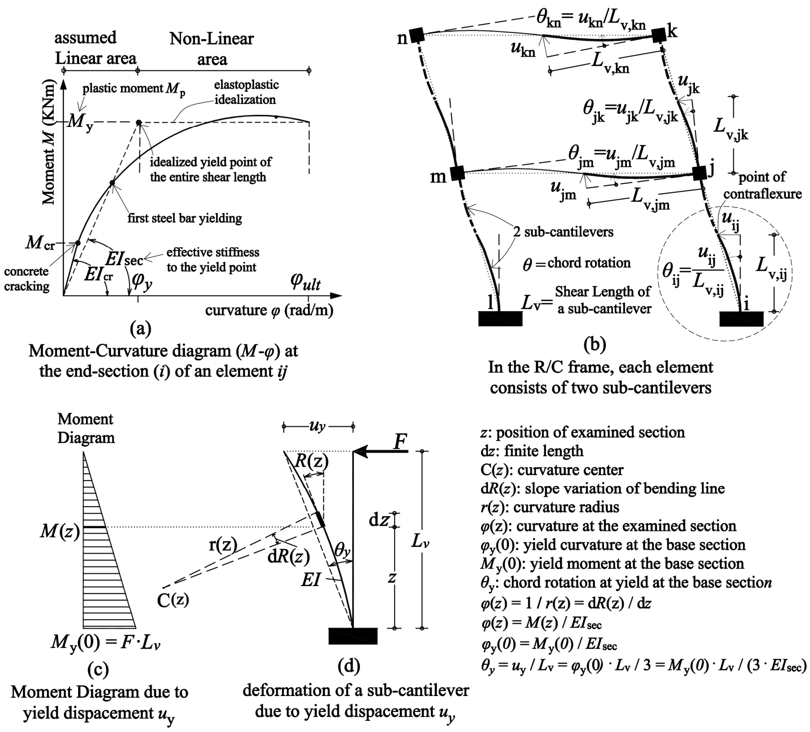

Figure 5. Definition of the curvature φ_y, chord rotation θ_y, and secant (effective) stiffness EI_{sec} at yield (EN1998-3), at the base cross-section of a cantilever column with shear span length L_V.

As this is too conservative (even at the NC state as mentioned before), a scaling is proposed in Figure 4 when the pushover analysis targets other higher seismic performance levels, such as DL or SD or all the other intermediate ones. According to [34], at the DL state the value of $E_c I_{eff}$ is suggested to be equal to $2 \cdot E_c I_{eff,NC}$ and between $0.25 \cdot E_c I_g$ and $0.5 \cdot E_c I_g$ and at the SD state to be equal to the average of the corresponding ones at the NC and DL states. Another point in Equation (8) is that it provides different values of effective stiffness at various structural elements. To simplify this, the mean effective stiffness at the NC state is assigned to each structural RC element of the nonlinear model according to the proposed methodology. From the parametric investigation of various ductile, multistory RC frames, it was found that the mean values of θ_{pr} at the 1st yield, DL, SD, and NC states were about equal to 0.004, 0.007, 0.024, and 0.032 rad, respectively. The value for the NC state was determined considering the plastic hinge length according to EN 1998-3. This equation is presented below in the numerical example. It was also found that, at the NC state, the mean value of $I_{eff,i}/I_g$ (according to Equation (8)) between all the structural RC elements was about equal to 0.15. For the DL state, the value of $I_{eff,i}/I_g = 0.35$ is considered, which is more than double the NC value, and for the SD state, the value of $I_{eff,i}/I_g = 0.25$. Moreover, the effective stiffness scenario of Figure 4 proposes discrete $I_{eff,i}/I_g$ values from the uncracked (health) state towards the 1st yield (when the 1st plastic hinge is shown) and from there to the DL. At 1st yield, the value of $I_{eff,i}/I_g = 0.50$ for elastic analysis is considered according to EN 1998-1 [37]. Additionally, two proposed lines (with the corresponding equations, where θ_{pr} is in rad units) for the effective stiffness ratio into the linear and nonlinear area are also presented in Figure 4 and fit the abovementioned proposed θ_{pr} and $I_{eff,i}/I_g$ values for the 1st yield, DL, SD, and NC states:

For the linear area, $0 \leq \theta_{pr} \leq 0.004$:

$$I_{eff}/I_g = 1 - 125 \cdot \theta_{pr} \tag{9}$$

For the nonlinear area, $0.004 < \theta_{pr} \leq 0.032$:

$$I_{eff}/I_g = 3 \cdot 10^6 \cdot {\theta_{pr}}^4 – 253312 \cdot {\theta_{pr}}^3 + 7383.2 \cdot {\theta_{pr}}^2 - 93.773 \cdot \theta_{pr} + 0.747 \tag{10}$$

For the nonlinear area in the vicinity of (near) collapse, $0.032 < \theta_{pr}$:

$$I_{eff}/I_g = M_p \cdot L_v / \left(3 \cdot \theta_y \cdot E_c \cdot I_g\right) \tag{11}$$

(d) The known fundamental eigenfrequency of the damaged structure of phase (a), f_1, is inserted in the instantaneous eigenfrequencies diagram (Figure 2) and, hence, the respective inelastic seismic (target) roof displacement u_i is determined. All the rest of the instantaneous higher eigenfrequencies $\left(f_{2,i}, f_{3,i}, \ldots f_{N,i}\right)$ of the existing damaged planar RC frame lie on the same vertical line passing through the target displacement u_i.

(e) The damage state of the structure can be identified by the results of two pushover analyses (with floor forces along the positive and negative directions) targeting the already known seismic roof displacement u_i found in the previous phase. Two sets of pushover analysis are performed, where the floor forces are applied according to the two patterns discussed in phase (b). The location and the state of the plastic hinges at the last step of each pushover analysis indicate an estimation of the damaged state of the existing RC frame structure, while the final requested damaged state of the structure will result from the envelope of the damage states of the two pushover sets.

(f) Moreover, a linear modal analysis is performed at the last step of each pushover analysis of phase (e), using as initial conditions the instantaneous stiffness matrix of the planar RC frame structure at this last pushover analysis step. From this instantaneous modal analysis, all the circular eigenfrequencies $\omega_{i,g}$ and all the mode shapes $\boldsymbol{\varphi}_{\mathrm{i,g}}$ of the damaged structure are calculated.

(g) At the end, the instantaneous stiffness matrix $\mathbf{k}_i$ of the planar RC frame structure is calculated at the examined inelastic *i*-step where the roof displacement u_i occurs. This can be achieved easily after the calculation of the flexibility matrix of the damaged frame structure at the same i-step. For this purpose, separate linear analyses with lateral forces applied sequentially on each floor, i.e., along the dynamic degrees of freedom of the frame, are performed at the last step of the pushover analyses of phase (e). Next, the stiffness matrix $\mathbf{k}_i$ of the damaged frame is calculated by inversing the flexibility matrix. Hence, the damage stiffness matrix $\Delta\mathbf{k}_i$ at the same inelastic *i*-step is calculated from the general relationship $\Delta\mathbf{k}_i = \mathbf{k}_o - \mathbf{k}_i$, where $\mathbf{k}_o$ is the known initial stiffness matrix of the undamaged frame structure, which is calculated at the health state as mentioned above.

The present methodology on multistory, planar, ductile RC frames that uses the hybrid M and P technique is deployed in the flowchart of Figure 6.

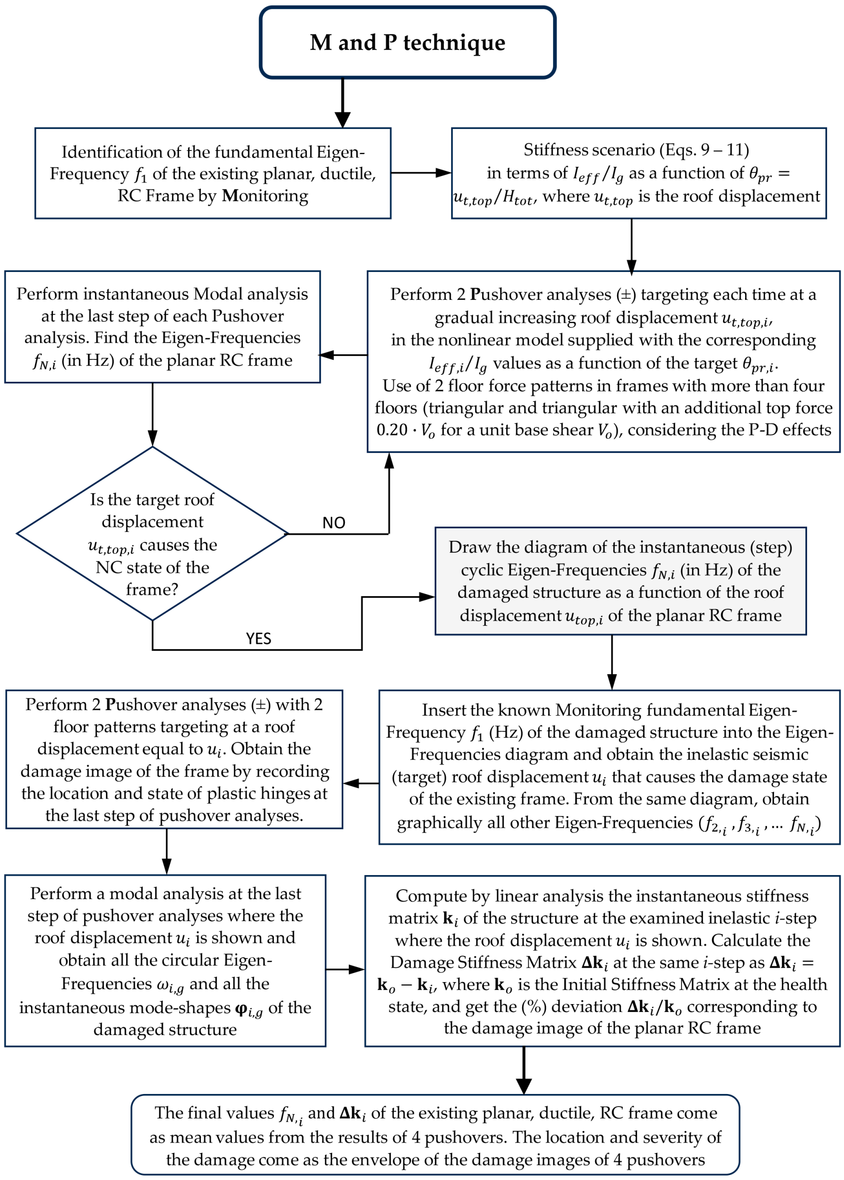

Figure 6. Flowchart of the hybrid P and M technique for damage identification in planar RC frames.

3. Numerical Example

We consider the existing five-story planar RC frame of Figure 7, with three unequal spans, with the dimensions $L_1 = 3.5$ m, $L_2 = 5.5$ m, and $L_3 = 4.5$ m. The story height is equal to 3.5 m on all floors, and the total height of the frame is 17.5 m. The total vertical uniformly distributed loads of the seismic combination $p = g + \psi_E q$ (where g is the dead load, $\psi_E q$ is the quasi-live load, and $\psi_E = 0.3$ [24]) applied on the spans of each floor are, respectively, equal to $p_1 = 28$, $p_2 = 35$, and $p_3 = 32$ kN/m. These loads contribute to a floor mass of approximately 45 tn and to a total frame mass of 225 tns. The floor mass and the degrees of freedom of the five-story planar frame for the modal analysis are illustrated in Figures 7b and 8b. Additionally, Figures 7a and 8a present the two patterns (P-1 and P-2) of lateral floor forces that are used in the pushover analysis. The frame was constructed with concrete grade C25/30 and steel grade B500s, with mean compressive and tensile strengths equal, respectively, to $f_{cm} = 33$ MPa and $f_{ym} = 550$ MPa. The elasticity modulus of the concrete is equal to $E_c = 31$ GPa, while that of the steel is $E_s = 200$ GPa. There are two different column sections, with dimensions $b_c \times h_c$ equal to 0.45×0.45 and 0.50×0.50 m, respectively. All the column sections are symmetrically reinforced with 12 steel bars of a 20 mm diameter (or 12Ø20) at all floors, except the top floor where the total steel bars are 4Ø20 + 8Ø14 (Figure 9). The confinement reinforcement in all the columns, on every floor, consists of closed hoops with four ties of an 8 mm diameter, evenly spaced per 8 cm axially at the critical end sections. The beams of the frame have a rectangular section of dimensions $b_b \times h_b = 0.30 \times 0.60$ m and are symmetrically reinforced at the upper and the lower fibers but have different steel bars on the various floors (Figure 9). The beams on all floors have a perimetric closed hoop of an 8 mm diameter, evenly spaced per 8 cm axially at the critical end sections, which acts as shear reinforcement and provides a low confinement state. The steel reinforcement details of the typical column and beam sections are shown in Figure 10. It is worth noting that the planar RC frame has been designed according to EN 1998-1 [37] for the high ductility class (DCH); hence, it is expected to demonstrate a beam-sway plastic mechanism in the nonlinear area.

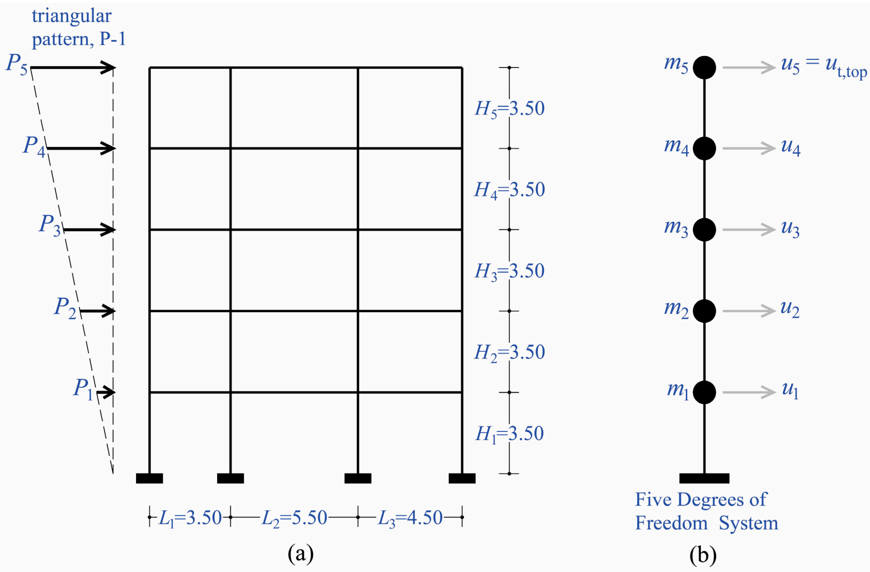

Figure 7. Five-story planar RC frame with three unequal spans: (**a**) static simulation for the first pushover set (P-1) with a triangular force pattern, (**b**) dynamic simulation.

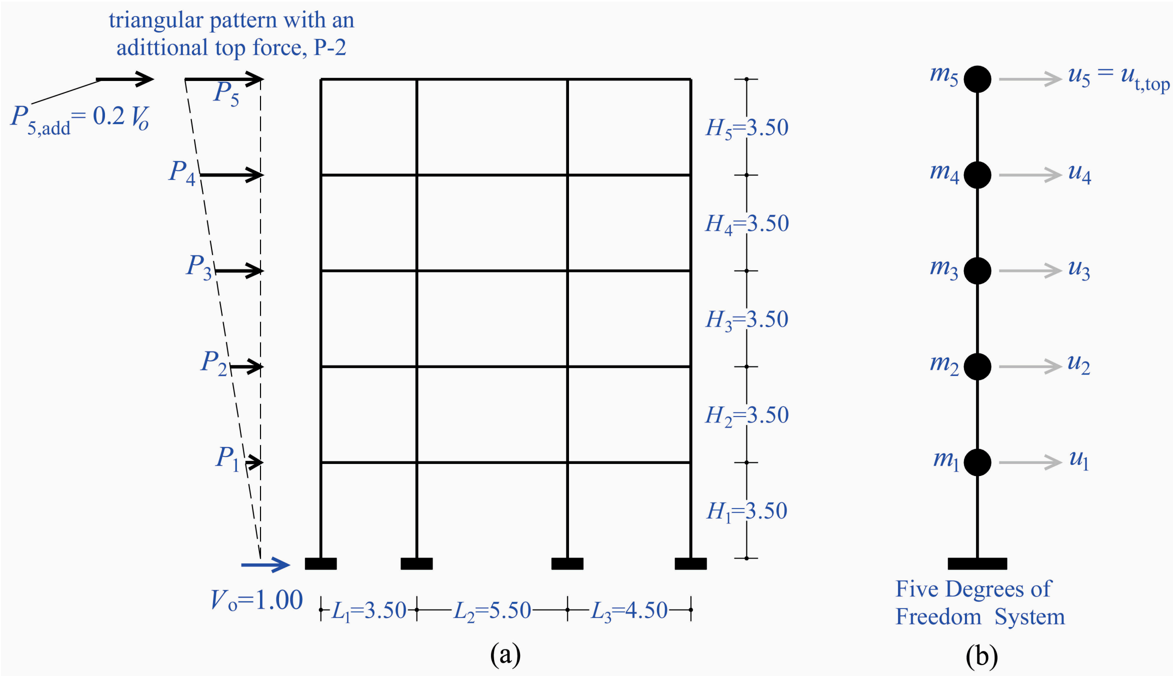

Figure 8. (**a**) Static simulation of the five-story planar RC frame for the second pushover set (P-2) with a triangular force pattern and an additional top force, (**b**) dynamic simulation.

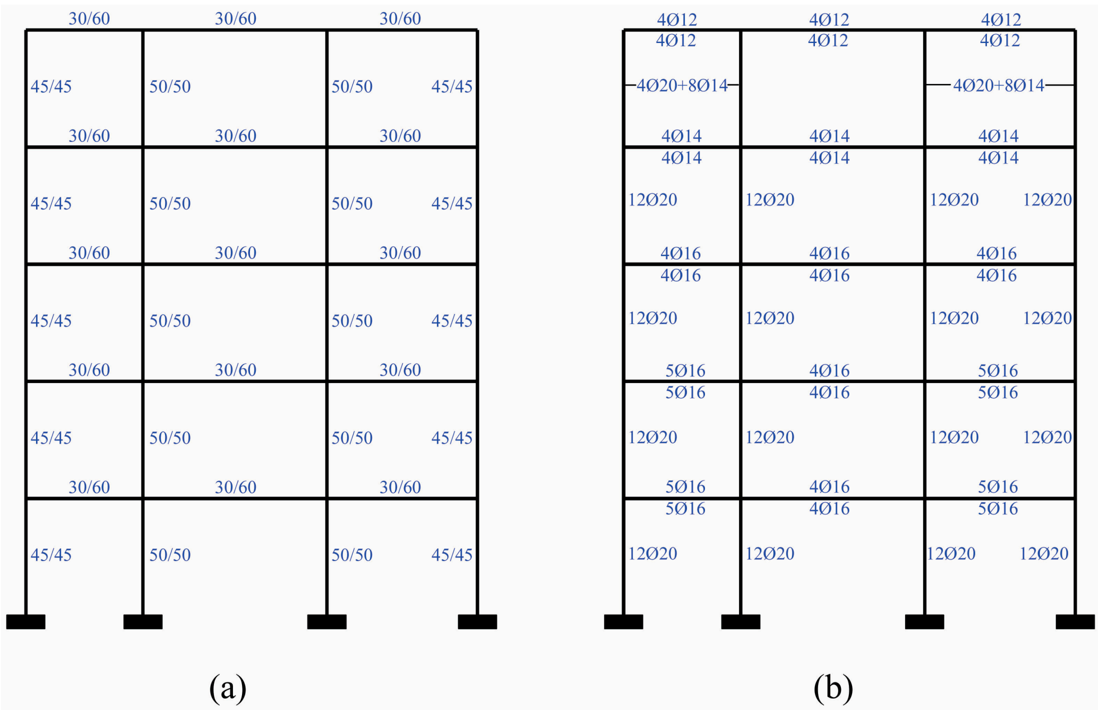

Figure 9. (**a**) Sections of RC structural elements, (**b**) longitudinal steel bars.

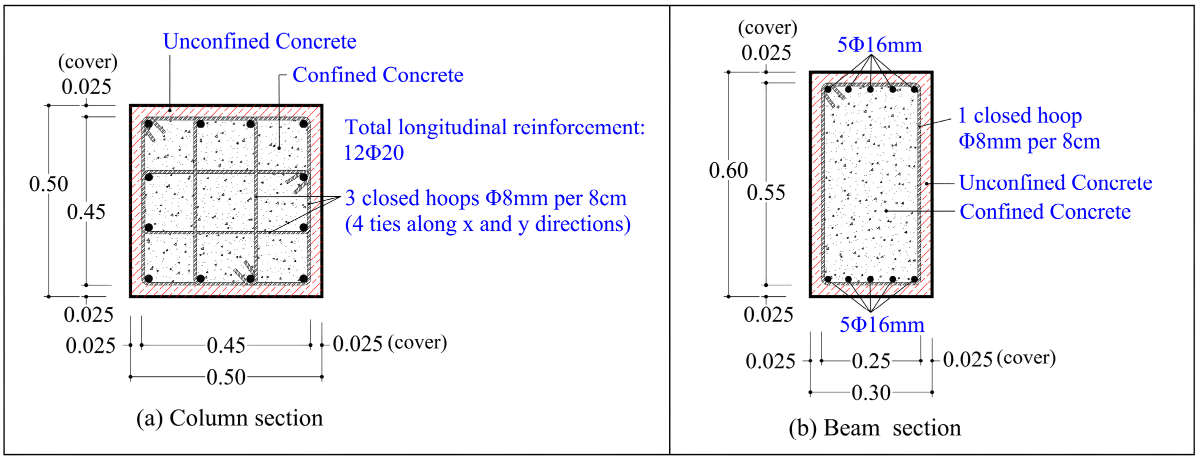

Figure 10. Steel reinforcement details of typical column and beam sections.

In order to apply the present methodology for the identification of the structural damage, a sequence of pushover and instantaneous modal analyses should be performed. The nonlinear model of the planar RC frame was created in the FEM analysis software SAP2000 [38] using fiber hinges to simulate the locations of the possible developing plastic hinges at the end sections of the elements, with the plastic hinge length calculated by Equation (A.9) of EN 1998-3 [35]:

$$L_{\mathrm{pl}} = \frac{L_{\mathrm{v}}}{30} + 0.2 \cdot h + 0.11 \cdot \frac{d_{\mathrm{bL}} \cdot f_{\mathrm{ym}}}{\sqrt{f_{\mathrm{cm}}}} \tag{12}$$

where f_{cm} is the mean concrete compressive strength, f_{ym} is the mean yield stress of steel, d_{bl} is the mean diameter of the tension reinforcement, h is the depth of the cross-section, and L_{v} is the shear span.

The material constitutive relationships used in the nonlinear analyses are consistent with: (a) the uniaxial unconfined and confined model for the concrete proposed by Mander, Priestley, and Park (1988) [39] (Figure 11) and (b) the steel reinforcement model (parabolic at strain hardening region) proposed by Park and Paulay (1975) [40] (Figure 12).

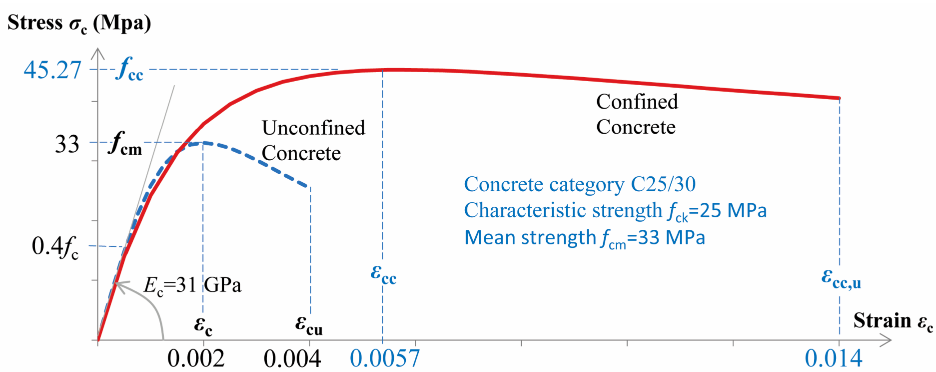

Figure 11. Stress–strain diagram for unconfined and confined concrete.

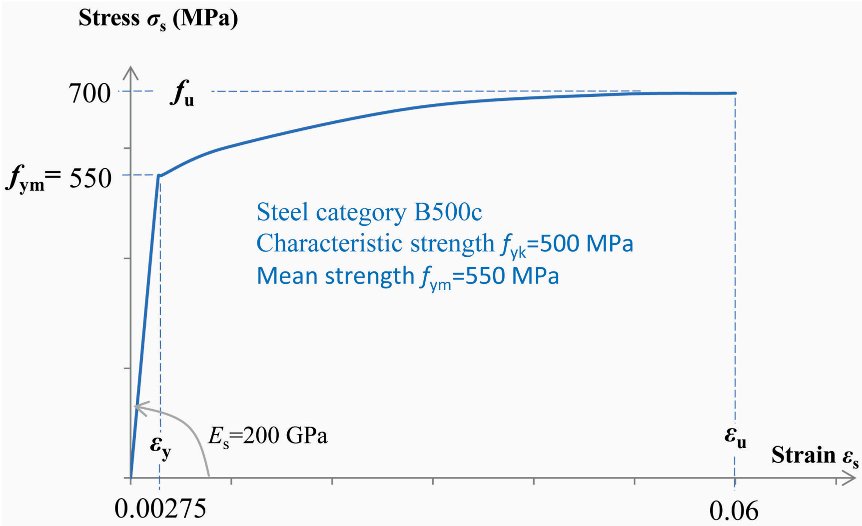

Figure 12. Stress–strain diagram for steel bars.

A section analysis [38] should be performed first in order to calculate the effective bending stiffness $E_c I_{\text{efff}}$ of the structural elements at the NC state, using Equation (8). Then, the stiffness scenario that will be used in the sequence of pushover analyses of the frame—with a gradually increasing (target) roof displacement—is established (phase c); this is presented in Table 1 as a function of the profile angle θ_{pr} (Figure 3). The discrete values of the effective moment of inertia I_{eff} assigned to all the RC structural elements of the nonlinear model of the frame depend on the seismic (target) roof displacement of the pushover analysis, i.e., on the target performance level (Figure 4). For example, if the target roof displacement $u_{t,top}$ corresponds to a value of θ_{pr} equal to 0.028, i.e., $u_{t,top} = \theta_{pr} \cdot H_{tot} = 0.028 \cdot 17.5 = 0.49$ m, then the I_{eff} value that should be assigned to all the RC structural elements of the nonlinear model is equal to $0.19 I_g$, as shown in Table 1.

Table 1. Effective moment of inertia ratio (I_{eff}/I_g) of RC structural elements as a function of the mean (chord) rotation of the frame structure θ_{pr} (rad).

θ_{pr}	I_{eff}/I_g	θ_{pr}	I_{eff}/I_g	θ_{pr}	I_{eff}/I_g	θ_{pr}	I_{eff}/I_g
0.000	1.00	0.010	0.32	0.020	0.28	0.030	0.17
0.001	0.87	0.011	0.32	0.021	0.27	0.031	0.16
0.002	0.74	0.012	0.31	0.022	0.26	0.032	0.15
0.003	0.61	0.013	0.30	0.023	0.25	*0.032+*	*Equation (8)*
0.004	0.50	0.014	0.30	0.024	0.24		
0.005	0.43	0.015	0.30	0.025	0.23		
0.006	0.40	0.016	0.30	0.026	0.22		
0.007	0.37	0.017	0.29	0.027	0.21		
0.008	0.35	0.018	0.29	0.028	0.19		
0.009	0.34	0.019	0.28	0.029	0.18		

To obtain the capacity curve of the planar frame, two pushover analyses are performed targeting the NC state, with the positive and negative signs of the floor lateral forces. In these analyses, the effective moment of inertia I_{eff} of Table 1 that corresponds to the NC state is used (Equation (8)), i.e., the value $0.15 I_g$. As the planar frame has more than four floors, two floor force patterns are used in the pushover analysis according to phase (b): (i) the triangular pattern (Figure 7a) and (ii) the triangular pattern but with an additional top force equal to $0.20 \cdot V_o$ for a unit base shear $V_o = 1.00$ kN (Figure 8a). These two force patterns are referred to, from now on, as P-1 and P-2. The four capacity curves of the planar frame for the two pushover sets are illustrated in Figure 13, together with the bi-linearization lines for the first set P-1, which mark the DL state at a value of θ_{pr}, which is about equal to 0.01 rad. As shown in this figure, the NC state of the frame is conservatively shown at a value of θ_{pr} equal to $0.567/17.5 = 0.032$ rad, i.e., that which is given in the last line of Table 1. The capacity curves for the second pushover set P-2 present higher ultimate displacements and lower elastic stiffness (effective stiffness K_{eff}, secant to the yield point), as is obvious in the figure. It is noted that the capacity curves that resulted from the pushover analyses that targeted other higher performance levels (for example SD or DL) do not present the same characteristics as those for the NC state. This is because of the different I_{eff} values which should be assigned to the structural elements in the nonlinear model to perform these pushovers.

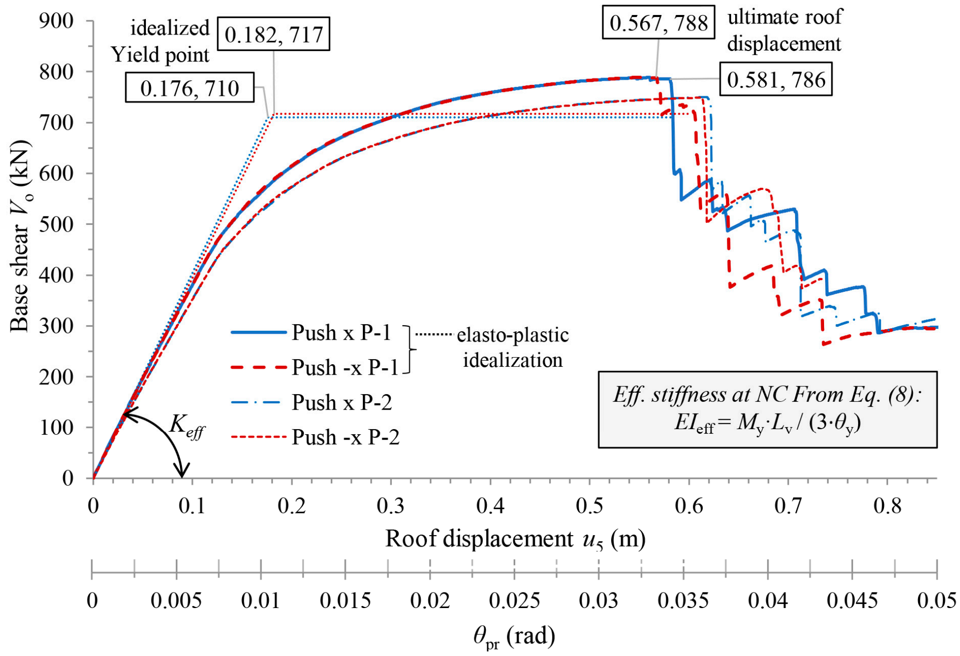

Figure 13. Capacity curves of the planar frame along the +x and -x axis (EI_{eff} at NC, Table 1), for the two force patterns P-1 and P-2.

Next, a sequence of pushover analyses of the existing planar frame is performed, where each one targets a seismic roof displacement which corresponds to the discrete values of the profile angle θ_{pr} of Table 1, from 0 to 0.032 rad. The first pushover analysis in the sequence is indeed for the zero lateral roof (target) displacement and includes only the action of the vertical loads of the seismic combination $g + \psi_E q$ in the health state. For this analysis, the value $I_{eff} = I_g$ is assigned to all the structural elements in the nonlinear model of the multistory RC frame. In all the other pushover analyses in the sequence, the effective moment of inertia I_{eff} assigned to the structural elements of the nonlinear model of the frame is that shown in Table 1, which corresponds to the same discrete values of the target profile angle θ_{pr}.

At the last step of the separate pushover analyses, an instantaneous modal analysis is run with the initial condition of the damage state of this last step, i.e., using the stiffness matrix of the damaged frame at the last step of each pushover analysis. From the sequence of modal analyses of the planar frame, the instantaneous cyclic eigenfrequencies of the system are recorded (F_1 to F_5), and the diagram of the instantaneous cyclic eigenfrequencies (in Hz) of the planar frame in the nonlinear area is obtained as a function of the roof displacement u_5 (Figure 14). This is conducted for both pushover sets, P-1 and P-2, where two pushover analyses are performed in each set with lateral floor forces along the positive and negative direction. Then, in order to obtain an assessment of the seismic damage of the existing multistory RC frame, the mean values of the instantaneous cyclic eigenfrequencies (in Hz) of the planar frame are calculated for each of the pushover sets P-1 and P-2. The cyclic eigenfrequencies (F_1 to F_5) that resulted from modal analysis at the last step of the positive and negatives pushovers of each of the pushover sets P-1 and P-2 are presented in Tables 2 and 3 for indicative values of θ_{pr}. The final values of the instantaneous cyclic eigenfrequencies (F_1 to F_5) are calculated as the mean of the results of the four pushovers of the two sets P-1 and P-2 and are presented in Table 4. As is obvious in this table, the instantaneous periods T_1 to T_5 (in sec) of the damaged frame (which are the inverse of the cyclic eigenfrequencies F_1 to F_5 in Hz) are elongated with increasing roof displacement. That is, the multistory RC frame becomes gradually more flexible due to the progress of the damage. This elongation of periods between the health state and the NC state is presented in Table 5. In Figure 14, the diagram of the instantaneous cyclic eigenfrequencies (in Hz) is combined with the capacity curve of the planar RC frame. The two diagrams are interconnected. This is the key figure of the proposed methodology in which:

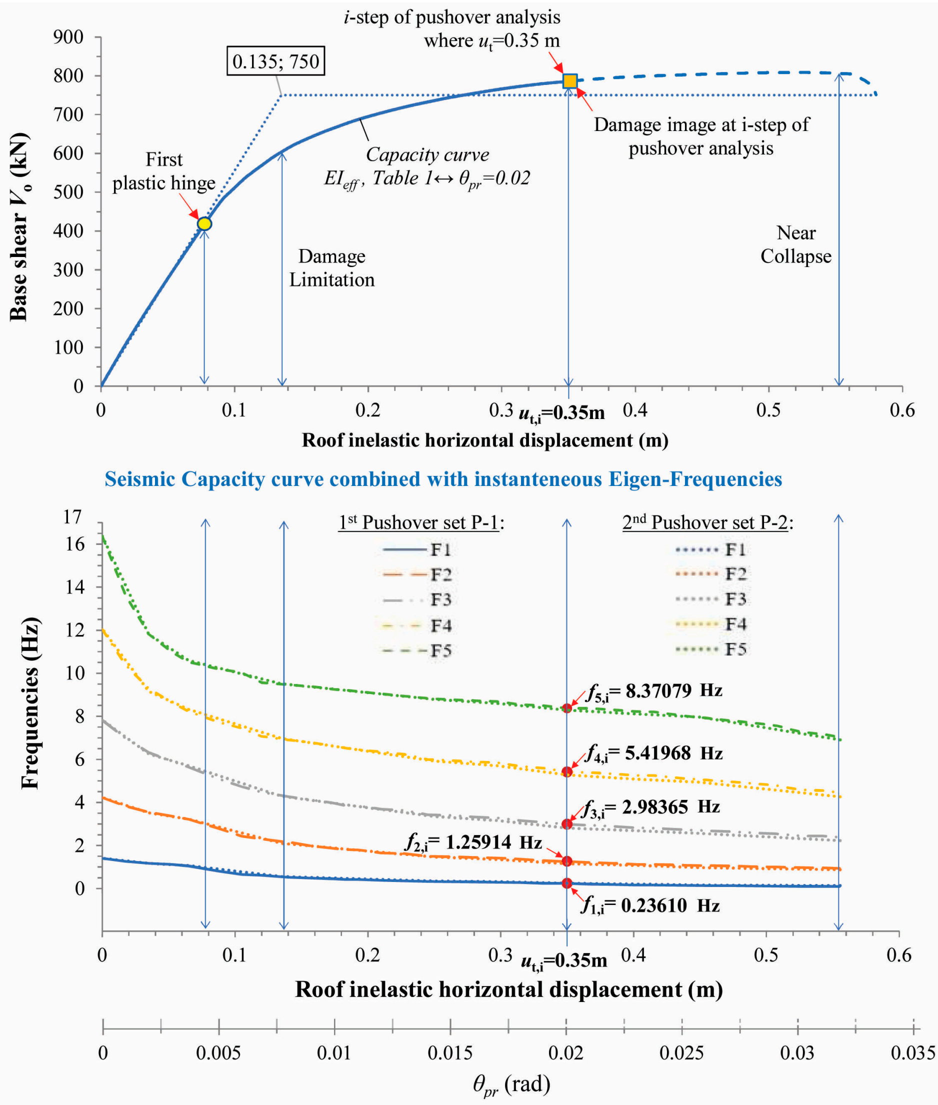

Figure 14. Diagram of the instantaneous eigenfrequencies in nonlinear area combined with the seismic capacity curve for the two pushover sets.

Table 2. Instantaneous cyclic eigenfrequencies (Hz) of the multistory frame for the P-1 pushover.

			Pushover P-1 with Positive Forces					Pushover P-1 with Negative Forces				
θ_{pr}	u_{top} (m)	I_{eff}/I_g	F_1	F_2	F_3	F_4	F_5	F_1	F_2	F_3	F_4	F_5
0.000	0.000	1.00	1.4042	4.2341	7.8406	12.1142	16.4007	1.4042	4.2341	7.8406	12.1142	16.4007
0.002	0.035	0.74	1.1752	3.5394	6.2924	9.2359	11.8190	1.1723	3.5451	6.3541	9.3505	11.8044
0.004	0.065	0.50	1.0423	3.2031	5.6383	8.2312	10.5222	1.0548	3.2278	5.6447	8.2191	10.5150
0.008	0.140	0.35	0.5305	2.1266	4.2647	6.9212	9.4692	0.5344	2.1940	4.2883	6.8960	9.4775
0.014	0.245	0.30	0.3300	1.4782	3.3848	5.9591	8.8240	0.3239	1.5040	3.4604	6.0385	8.8550
0.017	0.298	0.29	0.2959	1.4173	3.2962	5.8707	8.6991	0.2914	1.4140	3.2628	5.8233	8.6753
0.020	0.350	0.28	0.2299	1.2436	2.9720	5.4186	8.3651	0.2424	1.2747	2.9953	5.4207	8.3765
0.023	0.403	0.25	0.1610	1.1251	2.8189	5.2590	8.2050	0.1608	1.1230	2.8218	5.2585	8.2290
0.026	0.455	0.22	0.1340	1.0598	2.6771	5.0406	7.9014	0.1385	1.0663	2.6904	5.0423	7.9288
0.029	0.508	0.18	0.1136	1.0047	2.5454	4.7929	7.5615	0.1119	1.0062	2.5461	4.7872	7.5779
0.032	0.555	0.15	0.0891	0.9228	2.3469	4.4202	7.0015	0.1099	0.9642	2.4206	4.4998	7.0550

Table 3. Instantaneous cyclic eigenfrequencies (Hz) of the multistory frame for the P-2 pushover.

			Pushover P-2 with Positive Forces					Pushover P-2 with Negative Forces				
θ_{pr}	u_{top} (m)	I_{eff}/I_g	F_1	F_2	F_3	F_4	F_5	F_1	F_2	F_3	F_4	F_5
0.000	0.000	1.00	1.4042	4.2341	7.8406	12.1142	16.4007	1.4042	4.2341	7.8406	12.1142	16.4007
0.002	0.035	0.74	1.1806	3.5258	6.2758	9.1911	11.9099	1.1711	3.5147	6.2315	9.1269	11.6977
0.004	0.065	0.50	1.0545	3.1931	5.6845	8.3025	10.5969	1.0795	3.2542	5.7236	8.3419	10.6015
0.008	0.140	0.35	0.5578	2.1011	4.2880	6.9787	9.5029	0.5614	2.0878	4.2732	6.9612	9.5166
0.014	0.245	0.30	0.3582	1.5056	3.4200	6.0173	8.8449	0.3424	1.4288	3.2724	5.8288	8.7340
0.017	0.298	0.29	0.3271	1.3752	3.1978	5.7574	8.6387	0.3138	1.3364	3.1279	5.6588	8.5614
0.020	0.350	0.28	0.2402	1.1512	2.7924	5.2340	8.2582	0.2463	1.1532	2.8211	5.3157	8.3186
0.023	0.403	0.25	0.2134	1.0719	2.7094	5.1463	8.1527	0.2007	1.0744	2.6599	5.0168	8.0662
0.026	0.455	0.22	0.1524	0.9515	2.5397	4.9263	7.9696	0.1724	0.9968	2.5904	4.9431	7.9644
0.029	0.508	0.18	0.1556	0.9038	2.3453	4.5013	7.2607	0.1552	0.9118	2.3503	4.4819	7.2402
0.032	0.555	0.15	0.1379	0.8824	2.2328	4.2797	6.9233	0.1346	0.8697	2.2205	4.2454	6.8899

Table 4. Mean values of the instantaneous cyclic eigenfrequencies (Hz) of the multistory frame for the two pushover sets, P-1 and P-2.

θ_{pr}	u_{top} (m)	I_{eff}/I_g	F_1	F_2	F_3	F_4	F_5
0.000	0.000	1.00	1.4042	4.2341	7.8406	12.1142	16.4007
0.002	0.035	0.74	1.1748	3.5313	6.2884	9.2261	11.8078
0.004	0.065	0.50	1.0578	3.2195	5.6728	8.2737	10.5589
0.008	0.140	0.35	0.5460	2.1274	4.2785	6.9393	9.4916
0.014	0.245	0.30	0.3386	1.4792	3.3844	5.9609	8.8145
0.017	0.298	0.29	0.3071	1.3857	3.2212	5.7775	8.6436
0.020	0.350	0.28	0.2397	1.2057	2.8952	5.3473	8.3296
0.023	0.403	0.25	0.1840	1.0986	2.7525	5.1701	8.1632
0.026	0.455	0.22	0.1493	1.0186	2.6244	4.9881	7.9411
0.029	0.508	0.18	0.1341	0.9566	2.4468	4.6408	7.4101
0.032	0.555	0.15	0.1179	0.9098	2.3052	4.3613	6.9675

Table 5. Period (sec) elongation between the health state and the NC state.

	T_1	T_2	T_3	T_4	T_5
health state	0.71	0.24	0.13	0.08	0.06
NC	8.48	1.10	0.43	0.23	0.14

(a) From the diagram of eigenfrequencies, the roof seismic displacement u_i (or the corresponding θ_{pr} value) of the existing damaged RC frame is identified, after the insertion into the diagram of the monitoring fundamental frequency.

(b) At this roof seismic (target) displacement u_i, we are moving upwards to the capacity curve of the planar RC frame where we read the damage state visually.

The mean values of the cyclic eigenfrequencies that resulted from the two ($\pm$) pushovers of each pushover set are presented in this figure. For the figure's clarity, only one capacity curve is presented, that for the pushover with positive floor forces following a triangular pattern (P-1). This curve was determined using a nonlinear model of the frame in which the I_{eff} value of Table 1 that corresponds to $\theta_{\text{pr}} = 0.02$ rad has been assigned to all the RC structural elements, i.e., the value 0.28. As is shown in Figure 14, the two pushover sets P-1 and P-2 provide similar results for the instantaneous cyclic eigenfrequencies in this planar frame. At $\theta_{\text{pr}} = 0.02$ rad, the second pushover set (P-2) provides a (mean) value for f_1 (Hz) which is 3% higher, while for the other frequencies lower (mean) values of up to 8% are shown. Generally speaking, the difference for f_1 (Hz) increases linearly with the damage state for the second pushover set, up to 30% at the NC state. Finally, the mean values of the instantaneous cyclic eigenfrequencies (Hz) of the multistory frame that resulted from the four pushovers along the positive and negative directions (P-2 and P-3) should be used in the diagram (Table 4).

According to phase (a) of the methodology for the existing structures, an identification multichannel system of uniaxial accelerometers is installed in the five-story planar RC frame, and the response accelerations when the frame is quasi-calm are recorded. From the analysis of the records, the fundamental eigenfrequency $f_{1,i} = 0.23610$ Hz for the *i*-step of the pushover analysis is determined.

Then, according to phase (d) of the methodology, the fundamental eigenfrequency $f_{1,i}$ is inserted in the eigenfrequencies diagram of Figure 14 (see also the key in Figure 2), and the respective displacement $u_{5,i} = 0.35$ m of the frame roof is determined, which corresponds to $\theta_{pr} = 0.02$ rad. All the other higher frequencies ($f_{2,i}$ to $f_{5,i}$) can also be found from Figure 14 at the same *i*-step. The first three instantaneous mode shapes ($\varphi_{1,\text{i}}$ to $\varphi_{3,\text{i}}$) of the multistory frame at the corresponding *i*-step where θ_{pr} is equal to 0.02 rad are illustrated in Figure 15. Moreover, at the last step of the pushover analyses where the roof displacement $u_{5,i}$ appears, two damage images are obtained, one for the positive and one for the negative application of the floor forces, for each one of the two pushovers sets P-1 and P-2. From these two damage images for each of the pushover sets and by taking the envelope damage image from the two sets, the final requested estimation of the damage is obtained. In Figure 16, the damage images for the first pushover set P-1 are shown separately for the positive and negative directions of the lateral floor forces. In this figure, the developed plastic hinges are illustrated with a black semicircle at the upper or lower fibers of the beams. As shown in this figure, the multistory planar frame develops a beam-sway-type plastic mechanism, with plastic hinges at the end sections of the beams on all the floors (except the top floor) and at the base of the columns of the ground floor. This is fully in line with the seismic design objective for high ductility [37]. For the second set, P-2, of the pushover analysis, the damage is distributed throughout the frame, at the end sections of the beams on all the floors, but the magnitude of the damage is a little higher in the upper half of the frame and a little lower in the lower half (Figure 17). Also, no plastic hinges appear at the base of the columns of the ground floor.

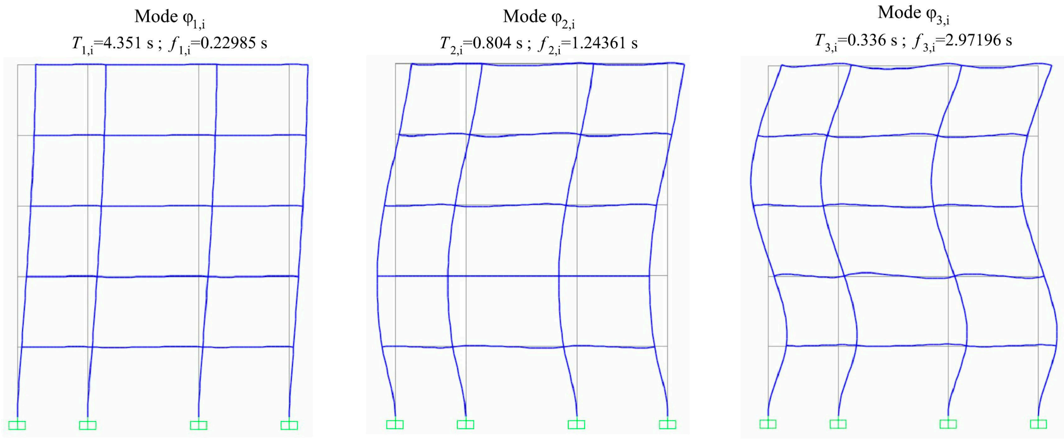

Figure 15. The first three instantaneous modes $\varphi_{1,\mathrm{i}}$ to $\varphi_{3,\mathrm{i}}$ at $\theta_{pr} = 0.02$ rad.

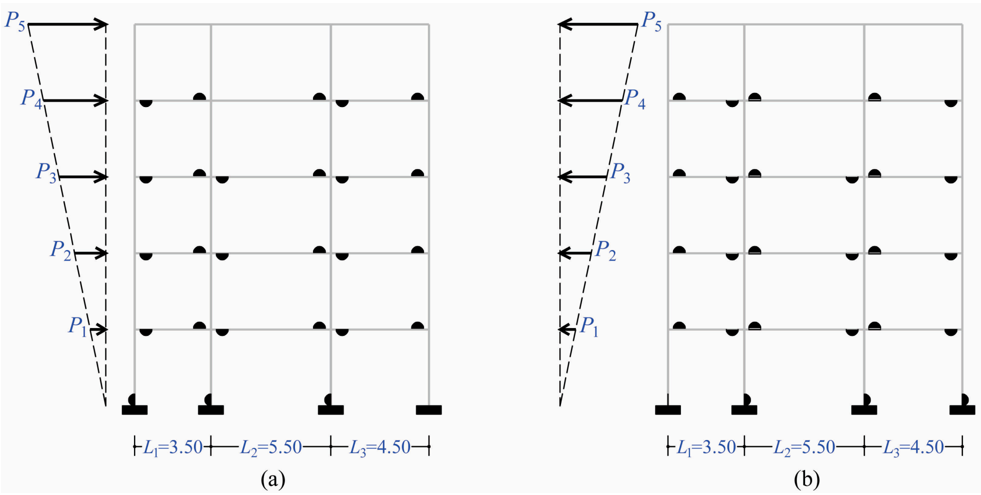

Figure 16. Plastic mechanism of the planar RC moment frame from the 1st set P-1 of pushover analysis, with (**a**) positive and (**b**) negative signs of floor forces, at seismic (target) displacement 0.35 m ($\theta_{pr} = 0.02$ rad) corresponding to the fundamental eigenfrequency of the damaged frame. Evaluation of damage locations.

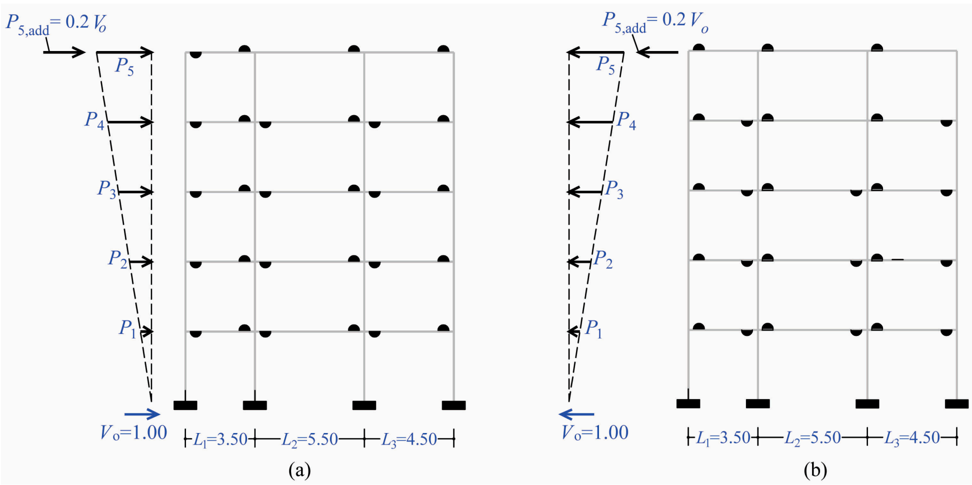

Figure 17. Plastic mechanism of the planar RC moment frame from the 2nd set P-2 of pushover analysis, with (**a**) positive and (**b**) negative signs of floor forces, at seismic (target) displacement 0.35 m ($\theta_{pr} = 0.02$ rad) corresponding to the fundamental eigenfrequency of the damaged frame. Evaluation of damage locations.

It is worth noting that in an earthquake event, the actual seismic load on the structure is different and that this loading varies in each time step. Hence, the damage distribution on the frame can be different from that obtained by the pushover analysis. However, the critical parameter in the recently proposed methodology is the fundamental eigenfrequency, which is identified through monitoring with a local network of uniaxial accelerometers. Knowing the fundamental eigenfrequency of the structure, the equivalent lateral displacement of the monitoring point on the roof of the building can be estimated, as shown in Figure 14; then, the capacity curve is considered to identify the damage state. On the other hand, the second set of pushover analyses, with the load pattern with an additional top force, should always be considered in tall moment frames with more than four floors, to take account of the higher mode effects on the damage potential. In this frame, both pushover sets provide similar values for the fundamental instantaneous cyclic eigenfrequency $f_{1,i}$ and for the damage image but, if the frame had been taller, then these results might have been different.

Finally, according to phase (g) of the methodology, the instantaneous stiffness matrix $\mathbf{k}_i$ of the frame structure at the examined inelastic i-step ($\theta_{pr} = 0.02$ rad) is calculated for the case of pushover analysis with positive floor forces following the triangular pattern (P-1):

$$\mathbf{k}_i = \begin{bmatrix} 36370.51 & -33082.10 & 14643.09 & -3673.87 & 679.84 \\ -33082.10 & 50479.70 & -38748.17 & 15118.43 & -2690.79 \\ 14643.09 & -38748.17 & 52466.20 & -36198.25 & 10206.16 \\ -3673.87 & 15118.43 & -36198.25 & 43966.32 & -19808.32 \\ 679.84 & -2690.79 & 10206.16 & -19808.32 & 11722.76 \end{bmatrix} \tag{13}$$

The above calculation is achieved easily at the last step of pushover analysis where the roof displacement $u_{5,i} = 0.35$ m appears, by calculating the flexibility matrix of the frame. For this purpose, five linear analyses with lateral unit forces applied each time on different floors (from the 1st to the 5th floor) are performed. Next, the stiffness matrix of the damaged frame is calculated by inversing the flexibility matrix.

Therefore, the damage stiffness matrix $\mathbf{\Delta k}_i$ at the same i-step is calculated from the general relationship $\mathbf{\Delta k}_i = \mathbf{k}_o - \mathbf{k}_i$, where $\mathbf{k}_o$ is the known initial stiffness matrix of the planar frame in the health state without damage. The latter can be calculated from the nonlinear model of the frame in which the geometric moment of inertia I_g has been assigned to all the RC structural elements, and the gravity loads are applied gradually:

$$\mathbf{k}_o = \begin{bmatrix} 257837.85 & -150932.01 & 37561.89 & -5540.92 & 712.70 \\ -150932.01 & 225406.70 & -140857.01 & 33129.35 & -3282.19 \\ 37561.89 & -140857.01 & 207019.25 & -118543.59 & 20706.76 \\ -5540.92 & 33129.35 & -118543.59 & 152434.25 & -62373.91 \\ 712.70 & -3282.19 & 20706.76 & -62373.91 & 44252.75 \end{bmatrix} \tag{14}$$

Hence, the damage stiffness matrix $\mathbf{\Delta k}_i$ of the planar frame, at the same i-step, is calculated as follows:

$$\begin{gathered} \mathbf{\Delta k}_i = \mathbf{k}_o - \mathbf{k}_i \\ = \begin{bmatrix} 221467.34 & -117849.92 & 22918.80 & -1867.05 & 32.86 \\ -117849.92 & 174926.99 & -102108.84 & 18010.92 & -591.40 \\ 22918.80 & -102108.84 & 154553.05 & -82345.34 & 10500.60 \\ -1867.05 & 18010.92 & -82345.34 & 108467.94 & -42565.59 \\ 32.86 & -591.40 & 10500.60 & -42565.59 & 32529.99 \end{bmatrix} \end{gathered} \tag{15}$$

For the pushover analysis with positive floor forces following the triangular pattern but with an additional top force (P-2), the corresponding damage stiffness matrix $\mathbf{\Delta k}_i$ of the planar frame, at the same i-step ($\theta_{\mathrm{pr}} = 0.02$ rad), is calculated as mentioned above and is equal to:

$$\mathbf{\Delta k}_i = \begin{bmatrix} 219118.62 & -117522.85 & 22932.98 & -1948.18 & 110.79 \\ -117522.85 & 175015.31 & -102488.80 & 18377.29 & -872.53 \\ 22932.98 & -102488.80 & 155574.83 & -84085.17 & 11567.50 \\ -1948.18 & 18377.29 & -84085.17 & 114674.18 & -47323.23 \\ 110.79 & -872.53 & 11567.50 & -47323.23 & 36434.37 \end{bmatrix} \quad (16)$$

4. Discussion

Considering Tables 2–4 for the eigenfrequencies, Figure 14 for the roof (target) displacement, Figures 16 and 17 for the plastic mechanism, as well as for the damage state, and the stiffness matrices (14–16) of the existing RC frame, the location and severity of the damage of the RC frame can now be confirmed in relation to the health state. This can be conducted since all the previous parameters are interrelated. This is the goal of the present work.

Indeed, knowing the damage stiffness matrix $\mathbf{\Delta k}_i$ of the planar frame, the final percentage deviation terms of $\mathbf{\Delta k}_i$ can be calculated with respect to the initial stiffness matrix $\mathbf{k}_o$, and they are presented in matrix form in Tables 6 and 7, respectively, for the P-1 and P-2 pushovers with positive floor forces. The visual representation of these tables is shown in Figures 18 and 19, respectively. These deviations on the diagonal terms of the damage stiffness matrix indicate the degree of damage of the planar five-story RC frame at the last step of pushover analysis where $\theta_{pr} = 0.02$ rad ($u_5 = 0.35$m) occurs, which is fully compatible with the damage images of Figures 16 and 17. The paper deals with damage in planar RC frames with a beam-sway plastic mechanism. In these frames, damage always occurs at the end sections of the beams of the various floors and not in the columns except at the base of the structure. It is noted that the diagonal terms of the stiffness matrix correspond to the lateral dynamic degrees of freedom of the floors of the planar frame (Figure 7). Therefore, the deviation of these terms in $\mathbf{\Delta k}_i$ corresponds to the overall damage of the beams of the various floors in planar RC frames that develop a plastic beam mechanism. For the ground floor, the corresponding first term of $\mathbf{\Delta k}_i$ also includes the damage at the base of the columns. We also notice that in Table 7 (P-2 pattern) the values of the terms in the damage stiffness matrix $\mathbf{\Delta k}_i$ that correspond to the upper half of the frame (degrees of freedom u_4, u_5) are higher, while those corresponding to the lower half of the frame (degrees of freedom u_1, u_2) are lower relative to the respective ones in Table 6 (P-1 pattern). The values of $\mathbf{\Delta k}_i$ that correspond to u_3 (intermediate floor) are about the same in both tables. Hence, the form as well as the values of the damage stiffness matrix $\mathbf{\Delta k}_i$ is fully compatible with the damage image in Figures 16 and 17. The final damage stiffness matrix $\mathbf{\Delta k}_i$, which marks the damage state of this planar RC frame, is determined as the average of the corresponding values resulting from the two patterns P-1 and P-2 (Figures 18 and 19).

Table 6. Percentage deviation of the damage stiffness matrix $\mathbf{\Delta k}_i$ at the i-step ($\theta_{pr} = 0.02$ rad) for the triangular force pattern (P-1).

Degrees of Freedom	u_1	u_2	u_3	u_4	u_5
u_1	85.89%	78.08%	61.02%	33.70%	4.61%
u_2	78.08%	77.61%	72.49%	54.37%	18.02%
u_3	61.02%	72.49%	74.66%	69.46%	50.71%
u_4	33.70%	54.37%	69.46%	71.16%	68.24%
u_5	4.61%	18.02%	50.71%	68.24%	73.51%

Table 7. Percentage deviation of the damage stiffness matrix $\mathbf{\Delta k}_i$, at the *i*-step ($\theta_{pr} = 0.02$ rad) for the triangular force pattern with an additional top force (P-2).

Degrees of Freedom	u_1	u_2	u_3	u_4	u_5
u_1	84.98%	77.86%	61.05%	35.16%	15.54%
u_2	77.86%	77.64%	72.76%	55.47%	26.58%
u_3	61.05%	72.76%	75.15%	70.93%	55.86%
u_4	35.16%	55.47%	70.93%	75.23%	75.87%
u_5	15.54%	26.58%	55.86%	75.87%	82.33%

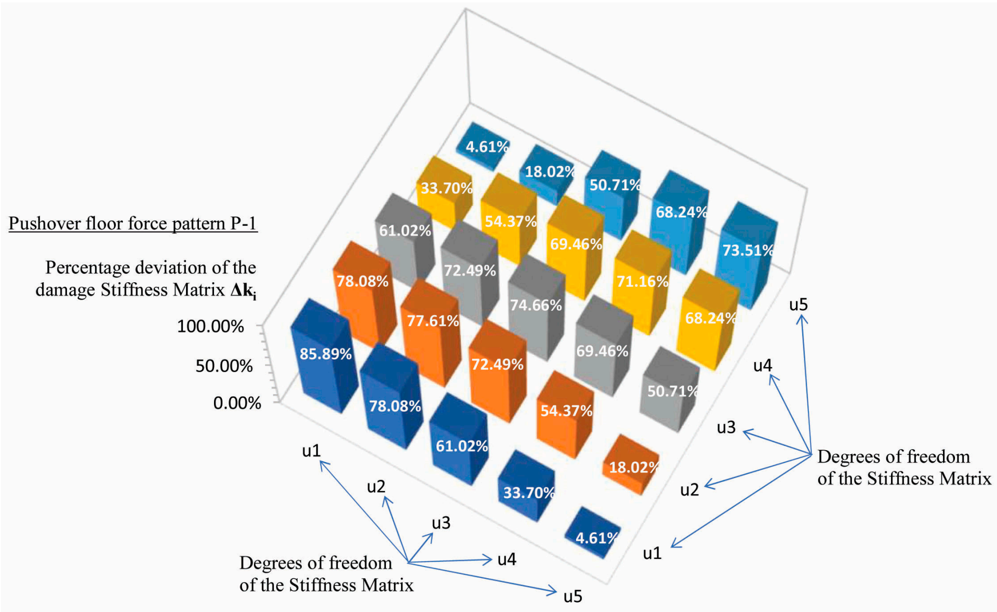

Figure 18. Percentage deviation of the damage stiffness matrix $\mathbf{\Delta k}_i$ at the *i*-step ($\theta_{pr} = 0.02$ rad) for the triangular force pattern (P-1).

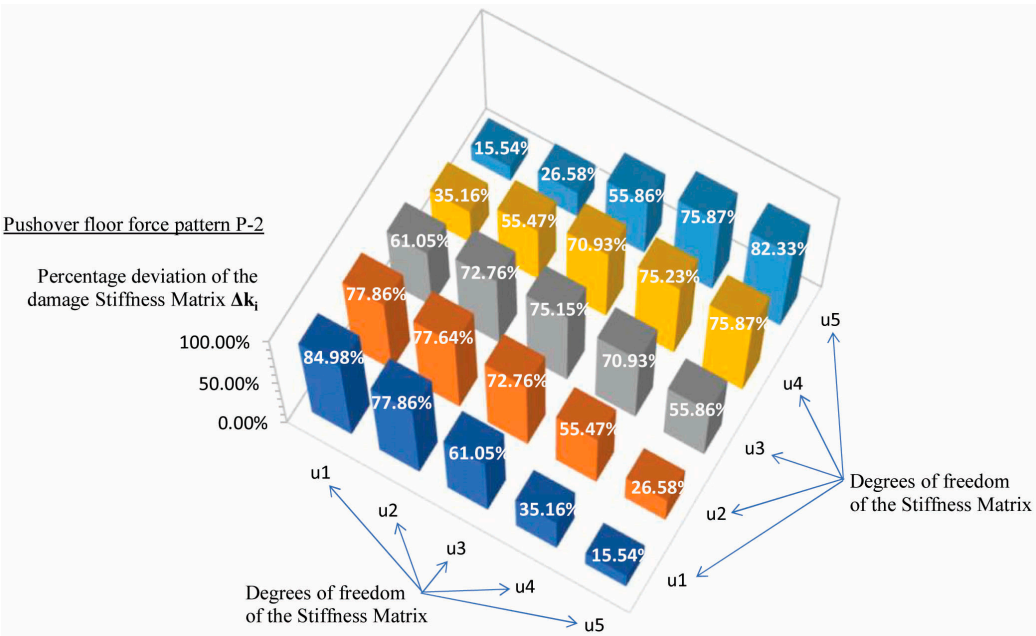

Figure 19. Percentage deviation of the damage stiffness matrix $\mathbf{\Delta k}_i$ at the *i*-step ($\theta_{pr} = 0.02$ rad) for the triangular force pattern with an additional top force (P-2).

Therefore, it is shown that for a given damage image in an existing, ductile, RC frame structure, the stiffness matrix of the healthy state of the structure changes, resulting in a change in the eigenfrequencies of the structure which are identified experimentally by the monitoring procedure. Then, using the key diagram of the method, the seismic roof displacement of the building is determined, which, on the one hand, corresponds to the damage image and, on the other hand, ensures the same values of the eigenfrequencies as those measured in the field. All the parameters used in the hybrid M and P technique are interrelated; hence, it is a self-evident and accurate process. This is clearly stated in the Methodology section.

5. Conclusions

A recently proposed methodology [33] for the identification of damage in RC frame structures is validated in the present paper by examining a group of planar, ductile, multistory RC moment frames, from which a numerical example was presented here. This is a five-story planar moment frame with three unequal spans which develops a beam-sway plastic mechanism. The methodology uses a hybrid technique, which is called the "M and P technique" (where M means "Monitoring" and P means "Pushover"), where the pushover capacity curve of the multistory frame is combined with the diagram of the instantaneous eigenfrequencies of the structure as a function of the inelastic seismic (target) roof displacement. This diagram was the result of performance of a sequence of pushover and instantaneous modal analyses with a gradually increasing target displacement $u_{top,i}$, which corresponded to a specific value of the mean (chord) rotation $\theta_{pr,i}$ of the moment frame. In each analysis, the RC structural elements of the nonlinear model are supplied with the appropriate values of the effective bending stiffness $E_c I_{eff,i}$ as a function of the target displacement, based on the concept of EN1998-3. By inserting in this diagram the fundamental eigenfrequency of the damaged frame identified by a monitoring network of accelerograms, the roof target displacement u_i of the frame arises and, hence, the damage image of the frame at the last step of the pushover analysis that targets this roof displacement u_i. Moreover, the instantaneous stiffness matrix and the damage stiffness matrix of the frame at the same last step of the pushover analysis is calculated. The latter is fully compatible with the degree of damage in the multistory frame at this last step of the pushover analysis, where the target displacement u_i is shown.

In this article, the pushover analysis was performed using two patterns of lateral floor forces (the second one with an additional top force) to account for the equivalent results due to the higher mode effects in the tall moment frames. Finally, all the results appear as the average of the four pushovers along the positive and negative direction while the final damage image is enveloped.

As all the parameters used in the hybrid M and P technique are interrelated (roof displacement, stiffness matrix, and eigenvalues) and based on the eigenfrequencies measured in the field by monitoring, the estimated damage image of the frame (location and severity) is always accurate. Therefore, using the present methodology for damage identification, a very good estimation of the distribution and of the magnitude of the damage in beam-sway, ductile, multistory, planar RC frames was achieved.

The M and P technique is suitable for damage identification in regular in-plan RC buildings consisting of RC frames that develop a beam-sway plastic mechanism and in regular in-plan dual buildings equivalent to wall buildings according to EN 1998-1. It is also suitable for such buildings that present moderate irregularities in elevation, but further investigation needs to be conducted for tall buildings with high irregular elevation. Moreover, the M and P technique can be used for damage detection in RC bridges, as it is an investigation currently being run by the authors. Also, the suitability of the technique in irregular in-plan RC buildings is investigated. Where the M and P technique cannot be applied is in RC buildings that develop a soft-story plastic mechanism, such as RC frame buildings designed without a capacity approach. A future investigation will also target the integration of the hybrid M and P technique in the health monitoring procedure of RC structures and in neural networks.

Author Contributions: Conceptualization, T.K.M. and A.P.B.; methodology, T.K.M.; software, T.K.M. and A.P.B.; validation, T.K.M. and A.P.B.; formal analysis, T.K.M. and A.P.B.; investigation, T.K.M. and A.P.B.; resources, T.K.M. and A.P.B.; data curation, T.K.M. and A.P.B.; writing—original draft preparation, A.P.B.; writing—review and editing, T.K.M. and A.P.B.; visualization, T.K.M. and A.P.B.; supervision, T.K.M.; project administration, T.K.M.; funding acquisition, none. All authors have read and agreed to the published version of the manuscript.

Funding: This research received no external funding.

Data Availability Statement: The data presented in this study are available in the article.

Conflicts of Interest: The authors declare no conflict of interest.

References

1. Basseville, M.; Benveniste, A.; Goursat, M.; Hermans, L.; Mevel, L.; Auweraer, H. Output-only Subspace-based structural identification: From theory to industrial testing practice. *J. Dyn. Syst. Meas. Control. Trans. ASME* **2001**, *123*, 668–676. [CrossRef]
2. Brincker, R.; Zhang, L.; Andersen, P. Modal identification of output-only systems using frequency domain decomposition. *Smart Mater. Struct. J.* **2001**, *10*, 441–445. [CrossRef]
3. Peeters, B. Identification and Damage Detection in Civil Engineering. Ph.D. Thesis, Katholieke Universiteit, Leuven, Belgium, 2000. Available online: https://www.researchgate.net/publication/238331491_System_Identification_and_Damage_Detection_in_Civil_Engineering (accessed on 1 September 2023).
4. Peeters, B.; Roek, G. Stochastic System Identification for Operational Modal Analysis: A Review. *J. Dyn. Syst. Meas. Control.* **2001**, *123*, 659–667. [CrossRef]
5. Wenzel, H.; Pichler, D. *Ambient Vibration Monitoring*; John Wiley & Sons, Ltd.: England, UK, 2005.
6. Overschee, P.; De Moor, B. *Subspace Identification for Linear Systems: Theory-Implemented-Applications*; Kluwer Academic Publishers: Dordrecht, The Netherlands, 1996. [CrossRef]
7. Papoulis, A. *Signal Analysis*; International Student Edition; McGraw-Hill Book: New York, NY, USA, 1985.
8. Oppenheim, A.; Schafer, R. *Digital Signal Processing*; Prentice-Hall, Inc., Publication: Englewood Cliffs, NJ, USA, 1999. Available online: https://research.iaun.ac.ir/pd/naghsh/pdfs/UploadFile_2230.pdf (accessed on 1 September 2023).
9. Bendat, J.; Piersol, A. *Random Data. Analysis and Measurement Procedures*, 4th ed.; John Wiley & Sons, Inc. Publication: Hoboken, NJ, USA, 2010. Available online: https://www.wiley.com/en-gb/Random+Data:+Analysis+and+Measurement+Procedures,+4th+Edition-p-9780470248775 (accessed on 1 September 2023).
10. Makarios, T. Identification of the mode shapes of spatial tall multi-storey buildings due to earthquakes. The new "modal time-histories" method. *J. Struct. Des. Tall Spec. Build.* **2012**, *21*, 621–641. [CrossRef]
11. Dragos, K.; Makarios, T.K.; Karetsou, I.; Manolis, G.D.; Smarsly, K. Detection and Correction of Synchronization-induced Errors in Operational Modal Analysis. *J. Arch. Appl. Mech. Springer* **2020**, *90*, 1547–1567. [CrossRef]
12. Zimmerman, D.C.; Kaouk, M. Structural damage detection using a minimum rank update theory. *J. Vib. Acoust.* **1994**, *116*, 222–231. [CrossRef]
13. Kaouk, M.; Zimmerman, D.C. Structural damage assessment using a generalized minimum rank perturbation theory. *AIAA J.* **1994**, *32*, 836–842. [CrossRef]
14. Domaneschi, M.; Limongelli, M.P.; Martinelli, L. Damage Identification in a benchmark Cable-Stayed Bridge using the Interpolation Method. In Proceedings of the 7th European Workshop on Structural Health Monitoring, La Cité, Nantes, France, 8–11 July 2014. Available online: https://www.researchgate.net/publication/281947001_Damage_Identification_in_a_Benchmark_Cable-StayedBridgeUsing_the_Interpolation_Method (accessed on 1 September 2023).
15. Domaneschi, M.; Limongelli, M.P.; Martinelli, L. Damage detection and localization on a Cable-Stayed Bridge. *Earthq. Struct.* **2015**, *5*, 1113–1126. [CrossRef]
16. Nazari, F.; Baghalian, S. A new Method for Damage Detection in symmetric beams using artificial neural network and Finite Element Method. *Int. J. Eng. Appl. Sci. (IJEAS)* **2011**, *3*, 30–36. Available online: https://dergipark.org.tr/en/pub/ijeas/issue/23578/251156 (accessed on 1 September 2023).
17. Amani, M.G.; Riera, J.D.; Curadelli, R.O. Identification of changes in the stiffness and damping matrices of linear structures through ambient vibrations. *Struct. Control. Health Monit. J.* **2007**, *14*, 1155–1169. [CrossRef]
18. Zhang, S.; Wang, H.; Wang, W.; Chen, S. Damage Detection in Structures Using Artificial Neural Networks. In Proceedings of the International Conference on Artificial Intelligence and Computational Intelligence, Sanya, China, 23–24 October 2010; pp. 207–210. Available online: https://ieeexplore.ieee.org/document/5656766 (accessed on 1 September 2023). [CrossRef]
19. Reuland, Y.; Martakis, P.; Chatzi, E. A Comparative Study of Damage-Sensitive Features for Rapid Data-Driven Seismic Structural Health Monitoring. *Appl. Sci.* **2023**, *13*, 2708. [CrossRef]

20. Martakis, P.; Reuland, Y.; Stavridis, A.; Chatzi, E. Fusing damage-sensitive features and domain adaptation towards robust damage classification in real buildings. *Soil Dyn. Earthq. Eng.* **2023**, *166*, 107739. [CrossRef]
21. Amini Pishro, A.; Zhang, Z.; Amini Pishro, M.; Xiong, F.; Zhang, L.; Yang, Q.; Matlan, S.J. UHPC-PINN-parallel micro element system for the local bond stress–slip model subjected to monotonic loading. *Structures* **2022**, *46*, 570–597. [CrossRef]
22. Amini Pishro, A.; Zhang, Z.; Amini Pishro, M.; Liu, W.; Zhang, L.; Yang, Q. Structural Performance of EB-FRP-Strengthened RC T-Beams Subjected to Combined Torsion and Shear Using ANN. *Materials* **2022**, *15*, 4852. [CrossRef]
23. Pishro, A.A.; Feng, X.; Ping, Y.; Dengshi, H.; Shirazinejad, R.S. Comprehensive equation of local bond stress between UHPC and reinforcing steel bars. *Constr. Build. Mater.* **2020**, *262*, 119942. [CrossRef]
24. Pishro, A.A.; Zhang, S.; Zhang, Z.; Zhao, Y.; Pishro, M.A.; Zhang, L.; Yang, Q.; Postel, V. Structural Behavior of FRP-Retrofitted RC Beams under Combined Torsion and Bending. *Materials* **2022**, *15*, 3213. [CrossRef]
25. Pishro, A.A.; Zhang, S.; Huang, D.; Xiong, F.; Li, W.; Yang, Q. Application of artificial neural networks and multiple linear regression on local bond stress equation of UHPC and reinforcing steel bars. *Sci. Rep.* **2021**, *11*, 15061. [CrossRef] [PubMed]
26. Lubrano Lobianco, A.; Del Zoppo, M.; Di Ludovico, M. Seismic Damage Quantification for the SHM of Existing RC Structures. In *Civil Structural Health Monitoring*; CSHM 2021. Lecture Notes in Civil Engineering; Rainieri, C., Fabbrocino, G., Caterino, N., Ceroni, F., Notarangelo, M.A., Eds.; Springer: Cham, Switzerland, 2021; Volume 156, pp. 177–195, ISBN 978-3-030-74257-7. [CrossRef]
27. Pepe, V.; De Angelis, A.; Pecce, M.R. Damage assessment of an existing RC infilled structure by numerical simulation of the dynamic response. *J. Civil. Struct. Health Monit.* **2019**, *9*, 385–395. [CrossRef]
28. Li, D.; Nie, J.H.; Wang, H.; Yan, J.B.; Hu, C.X.; Shen, P. Damage location, quantification and characterization of steel-concrete composite beams using acoustic emission. *Eng. Struct.* **2023**, *283*, 115866. [CrossRef]
29. Huang, H.; Guo, M.; Zhang, W.; Zeng, J.; Yang, K.; Bai, H. Numerical investigation on the bearing capacity of RC columns strengthened by HPFL-BSP under combined loadings. *J. Build. Eng.* **2021**, *39*, 102266. [CrossRef]
30. Cai, J.; Pan, J.; Li, G.; Elchalakani, M. Behaviors of eccentrically loaded ECC-encased CFST columns after fire exposure. *Eng. Struct.* **2023**, *289*, 116258. [CrossRef]
31. Huang, H.; Huang, M.; Zhang, W.; Guo, M.; Chen, Z.; Li, M. Progressive collapse resistance of multistory RC frame strengthened with HPFL-BSP. *J. Build. Eng.* **2021**, *43*, 103123. [CrossRef]
32. Guo, M.; Huang, H.; Zhang, W.; Xue, C.; Huang, M. Assessment of RC Frame Capacity Subjected to a Loss of Corner Column. *J. Struct. Eng.* **2022**, *148*, 9. [CrossRef]
33. Makarios, T. Damage Identification in plane multi-storey reinforced concrete frame. *Open Constr. Build. Technol. J.* **2023**, *17*, 1–10. [CrossRef]
34. Bakalis, A.; Makarios, T. Seismic Enforced-Displacement pushover procedure on multistorey R/C buildings. *Eng. Struct.* **2021**, *229*, 111631. [CrossRef]
35. *EN 1998-3*; Eurocode 8: Design of Structures for Earthquake Resistance—Part 3: Assessment and Retrofitting of Buildings. European Committee for Standardization: Brussels, Belgium, 2005.
36. Bakalis, A.; Makarios, T. Dynamic eccentricities and the "capable near collapse centre of stiffness" of reinforced concrete single-storey buildings in pushover analysis. *Eng. Struct.* **2018**, *166*, 62–78. [CrossRef]
37. *EN 1998-1*; Eurocode 8: Design of Structures for Earthquake Resistance—Part 1: General Rules, Seismic Actions and Rules for Buildings. European Committee for Standardization: Brussels, Belgium, 2004.
38. *Structural Analysis Program SAP2000v23*; Computers and Structures, Inc.: Walnut Creek, CA, USA, 2021; Available online: www.csiamerica.com (accessed on 1 September 2023).
39. Mander, J.B.; Priestley, M.J.N.; Park, R. Theoretical Stress-Strain Model for Confined Concrete. *J. Struct. Eng.* **1988**, *114*, 1804–1826. Available online: https://ascelibrary.org/doi/10.1061/%28ASCE%290733-9445%281988%29114%3A8%281804%29 (accessed on 1 September 2023). [CrossRef]
40. Park, R.; Paulay, T. *Reinforced Concrete Structures*; John Wiley & Sons, Inc.: New York, NY, USA, 1975.